THE JOURNAL OF PHYSICAL CHEMISTRY C

Article

pubs.acs.org/JPCC

Controlling Oxidation Potentials in Redox Shuttle Candidates for Lithium-Ion Batteries

Selin Ergun, Corrine F. Elliott, Aman Preet Kaur, Sean R. Parkin, and Susan A. Odom*

Department of Chemistry, University of Kentucky, Lexington, Kentucky 40506-0055, United States

Supporting Information

ABSTRACT: Overcharge, a condition in which cell voltage rises to undesirably high potentials, can be prevented in lithium-ion batteries by incorporating redox shuttles into the battery electrolyte. Although extensive overcharge protection has been demonstrated in batteries with $LiFePO_4$ cathodes, the redox shuttles that work in these batteries are incompatible with higher voltage cathodes. Designing stable additives with higher oxidation potentials is necessary to protect high voltage batteries from overcharge. Toward that goal, we synthesized diarylamines with varied structures, including fused heteroaromatic ring systems and electron-withdrawing substituents. We found that trends in oxidation potentials correlated with those in calculated adiabatic ionization potentials. Some diarylamine derivatives protected batteries from overcharge with varying degrees of success.

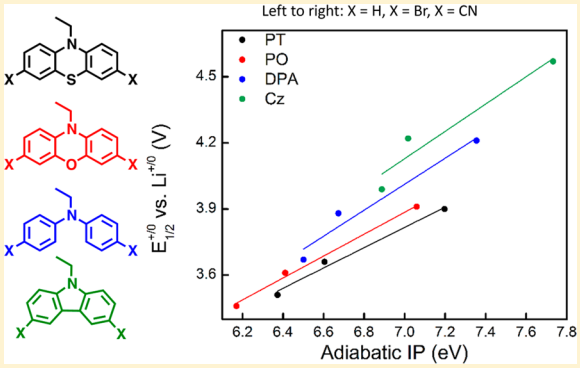

1. INTRODUCTION

Rechargeable lithium-ion batteries (LIBs) are common power sources for many portable electronic devices. Long battery lifetimes, lack of memory effect, and compatibility with modern electronics contribute to their widespread use.[1] The capability of LIBs to serve as high energy density sources has also led them to be used in larger scale applications, including hybrid electric vehicles, airplanes, and power tools.[2] Despite the advantageous characteristics that have led to their dominance in portable electronics, safety issues including fires in cars and airplanes, as well as in battery manufacturing plants, have raised concerns about their use in large-scale applications.[3]

One safety concern is overcharge, a condition that occurs when the normal operating voltage of a cell is exceeded,[4] as it can lead to increased cell temperatures when reactions occur at the electrode/electrolyte interface. For a single cell, the state of charge (SOC) can be monitored electronically and the current manipulated.[5,6] In series-connected cells, it is less practical to monitor the SOC of individual cells. An alternative approach to limiting charge in batteries connected in a series is to employ reversibly oxidizable chemical additives into the battery electrolyte.

Electrolyte additives called redox shuttles can prevent overcharge by serving as an electrical shunt, passing current along the series and preventing overcharge. Redox shuttles are oxidized at the cathode/electrolyte interface, ideally at the end-of-charge potential of the cathode, and then diffuse to the anode where reduction occurs, returning the redox shuttle to its neutral form.[7] Redox shuttles have been developed to match the end-of-charge potentials of $LiCoO_2$[8] and $LiFePO_4$ batteries, including 1,4-dimethoxy-2,5-bis(*tert*-butyl)benzene,[9] *N*-ethylphenothiazine,[10] and 2,2,6,6-tetramethylpiperidinyl oxide (TEMPO),[11] all of which protect for at least 100 cycles at 100% overcharge in $LiFePO_4$/graphite batteries but are limited in application to these lower (<4 V) batteries.[12]

Oxidation potentials can be varied with structural modifications, and radical cation stability can be increased by extending conjugation, substitution with electron-donating groups, or insertion of sterically hindered groups.[13] However, achieving both high oxidation potentials and stable oxidized (radical cation) species is a significant challenge. Introducing electron-withdrawing groups to increase oxidation potentials often further destabilizes the radical cation form by making it even more electron deficient, as is seen in the relatively few number of stable redox shuttles with high oxidation potentials. Tetraethyl-2,5-di-*tert*-butyl-1,4-phenylene diphosphate (4.80 V vs $Li^{+/0}$, >10 cycles, in $Li_{1.2}Ni_{0.15}Co_{0.1}Mn_{0.55}O_2$/Li batteries),[14] 2-(pentafluorophenyl)-tetrafluoro-1,3,2-benzodioxaborole (4.43 V vs $Li^{+/0}$, 178 cycles in graphite/$LiNi_{0.8}Co_{0.15}Al_{0.05}O_2$),[15] 1,4-di-*tert*-butyl-2,5-bis(2,2,2,-trifluoroethoxy)benzene (4.25 V vs $Li^{+/0}$, 98−170 cycles in MCMB/$LiFePO_4$ and $Li_4Ti_5O_{12}$/$LiFePO_4$ batteries),[16] 4-*tert*-butyl-1,2-dimethoxybenzene (4.18 V vs $Li^{+/0}$, 3−15 cycles in $Li_4Ti_5O_{12}$/$LiFePO_4$ and graphite/$LiFePO_4$ batteries),[17] 2,5-difluoro-1,4-dimethoxybenzene (4.4 V vs $Li^{+/0}$, 50 cycles in Li/$Li_4Ti_5O_{12}$ batteries, although very little charging capacity remains after 15 cycles),[18] and fluorodecaborate salts (4.5 V vs $Li^{+/0}$, 20 cycles in GDR/$LiNi_{0.8}Co_{0.15}Al_{0.05}O_2$)[19] are among the most robust higher voltage redox shuttles. For redox shuttles to be used with high voltage cathode materials such as $LiNi_{0.5}Mn_{1.5}O_4$ (4.9 V),

Received: April 17, 2014
Revised: June 14, 2014
Published: June 16, 2014

   dx.doi.org/10.1021/jp503767h | J. Phys. Chem. C 2014, 118, 14824−14832

$LiNiOSO_4$ (5.0 V), $LiNiSO_4F$ (5.2−5.4 V), and Li_2CoPO_4F (5.5 V), which can be charged to as high as 5.0 V or even higher,[14,20−23] it is necessary to develop stable redox shuttles with suitable oxidation potentials.

On the basis of the relatively large number of overcharge cycles reported for phenothiazines, in combination with the small number of derivatives tested as redox shuttles (mainly those in which the alkyl substituent on the *N*-position was varied), we synthesized and evaluated a series of phenothiazine derivatives and related compounds with diarylamine-based cores that could be synthesized in three or fewer steps from commercially available starting materials. Specifically, we incorporated electron-withdrawing substituents at the *para* positions of diarylamines to increase oxidation potentials and prevent dimerization reactions.[24,25] The oxidation of alkylated arylamines generates reactive sites on the radical cation, which undergoes irreversible coupling that can be followed by deprotonation.[13,24,26] The dimerization happens predominately at the positions *ortho* and *para* to the nitrogen atom due to the high electron spin density and absence of steric hindrance, although in some cases the *ortho* position may be less reactive due to steric hindrance to the alkyl groups.[24] Thus, for each aromatic core, we blocked the positions *para* to the N atom with Br atoms or cyano (CN) groups.

We also varied the heteroatom from phenothiazine (S) to phenoxazine (O) and also synthesized fused versions with no heteroatom (carbazole) and no fused ring (diphenylamine). We synthesized *N*-ethylated derivatives of these four cores, as shown in Figure 1. Here we report calculated adiabatic ionization potentials and experimentally determined oxidation potentials, diffusion coefficients, stability of the oxidized species in dilute solutions, and overcharge performance in lithium-ion batteries containing the diarylamines as electrolyte additives.

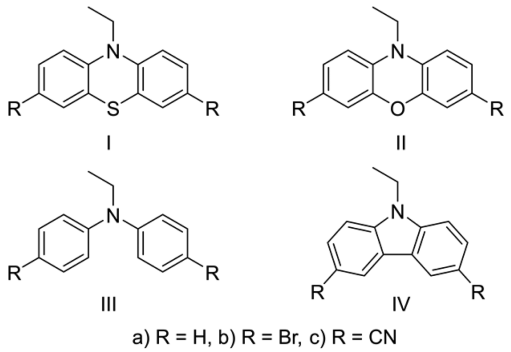

Figure 1. *N*-Ethylphenothiazine (**I**), *N*-ethylphenoxazine (**II**), *N*-ethyldiphenylamine (**III**), and *N*-ethylcarbazole (**IV**) derivatives with open *para* positions (a), bromine atoms (b), and cyano groups (c).

2. EXPERIMENTAL SECTION

General Experimental Section. *N*-Ethylphenothiazine (EPT), 3,7-dibromo-*N*-ethylphenothiazine (DBrEPT), and 3,7-dicyano-*N*-ethylphenothiazine (DCNEPT) were synthesized as previously reported.[27,28] Silica gel (63−200 μm) was purchased from Sorbent Technologies, and solvents for purification were purchased from Fisher Scientific. Sodium hydride and diphenylamine were purchased from Alfa Aesar. Bromoethane, phenothiazine, carbazole, and copper(I) cyanide were purchased from Sigma-Aldrich. Phenoxazine and *N*-bromosuccinimide (NBS) and the anhydrous solvents *N*,*N*-dimethylformamide, acetonitrile, and dichloromethane were purchased from Acros. Carbazole was freshly crystallized from hot acetone, and NBS from hot water, prior to use. All the other reagents were used without further purification. ^{1}H and ^{13}C NMR spectra were obtained on Varian spectrometers in DMSO-d_6 or $CDCl_3$ from Cambridge Isotope Laboratories. Mass spectra were recorded using an Agilent 5973 Network mass selective detector attached to Agilent 6890N Network GC system. Elemental analyses were performed by Atlantic Microlab, Inc.

Synthesis. The synthetic routes for the diarylamine derivatives are shown in Scheme 1. Disubstituted diarylamines were synthesized from commercially available phenothiazine, phenoxazine, diphenylamine, and carbazole. First, diarylamines were alkylated with bromoethane. *N*-Bromosuccinimide was used to brominate the resultant *N*-alkylated diarylamines. Coupling of the dibrominated derivatives with copper cyanide yielded the dicyano derivatives. The products were characterized by ^{1}H NMR, ^{13}C NMR, GCMS, and elemental analysis. Their electronic properties were studied by cyclic voltammetry and predicted with computational chemistry. We grew X-ray quality crystals for some of the compounds. We recently reported the EPT and DCNEPT crystal structures.[27,28] Synthetic procedures, characterization, and X-ray crystal structures of EPO, DBrEDPA, DCNEPO, DCNEDPA, and DCNECz are shown in the Supporting Information (Figure S1).

Cyclic Voltammetry. Cyclic voltammetry (CV) experiments were performed using a CH Instruments 600D potentiostat using a three-electrode system in 0.1 M nBu$_4$NPF$_6$ in dry acetonitrile (ACN) containing ca. 0.3 mM analyte.

Scheme 1. Synthetic Route Used To Synthesize *N*-Ethylphenothiazine (EPT), *N*-Ethylphenoxazine (EPO), 3,7-Dibromo-*N*-ethylphenothiazine (DBrEPT), 3,7-Dibromo-*N*-ethylphenoxazine (DBrEPO), 3,7-Dicyano-*N*-ethylphenothiazine (DCNEPT), 3,7-Dicyano-*N*-ethylphenoxazine (DCNEPO), *N*-Ethyldiphenylamine (EDPA), 4,4′-Dibromo-*N*-ethyldiphenylamine (DBrEDPA), 4,4′-Dicyano-*N*-ethyldiphenylamine (DCNEDPA), *N*-Ethylcarbazole (ECz), 3,6-Dibromo-*N*-ethylcarbazole (DBrECz), and 3,6-Dicyano-*N*-ethylcarbazole (DCNECz)

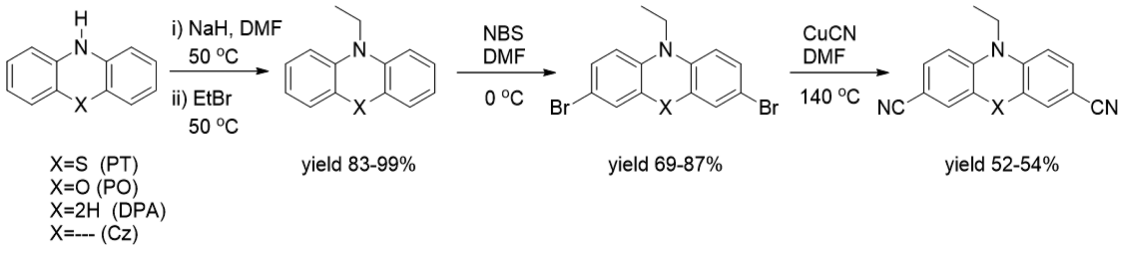

dx.doi.org/10.1021/jp503767h | J. Phys. Chem. C 2014, 118, 14824−14832

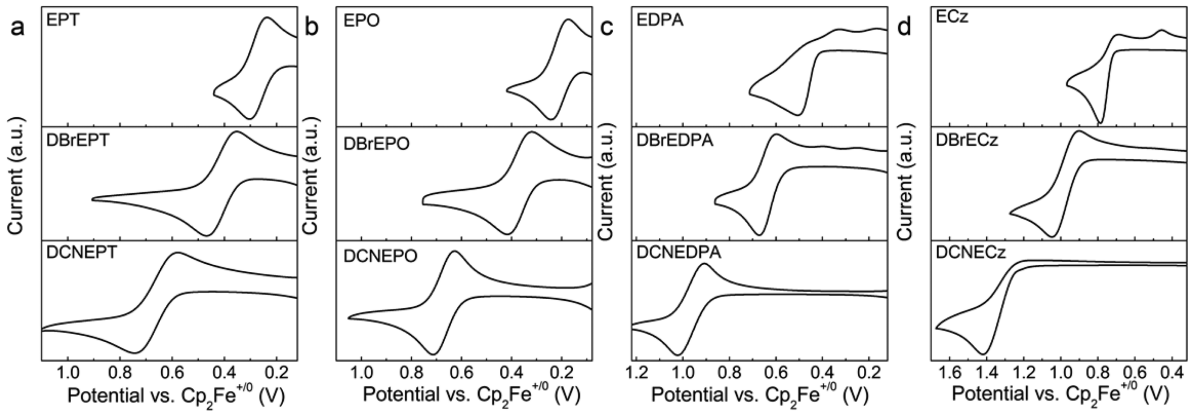

Figure 2. Cyclic voltammograms of EPT and its derivatives (a), EPO and its derivatives (b), EDPA and its derivatives (c), and ECz and its derivatives (d) at 0.3 mM in 0.1 M nBu$_4$NPF$_6$ in acetonitrile vs Cp$_2$Fe$^{+/0}$ at 0 V. All solutions contain Cp$_2$Fe as the internal reference (not shown, see Supporting Information for complete plots) and were recorded at 100 mV/s.

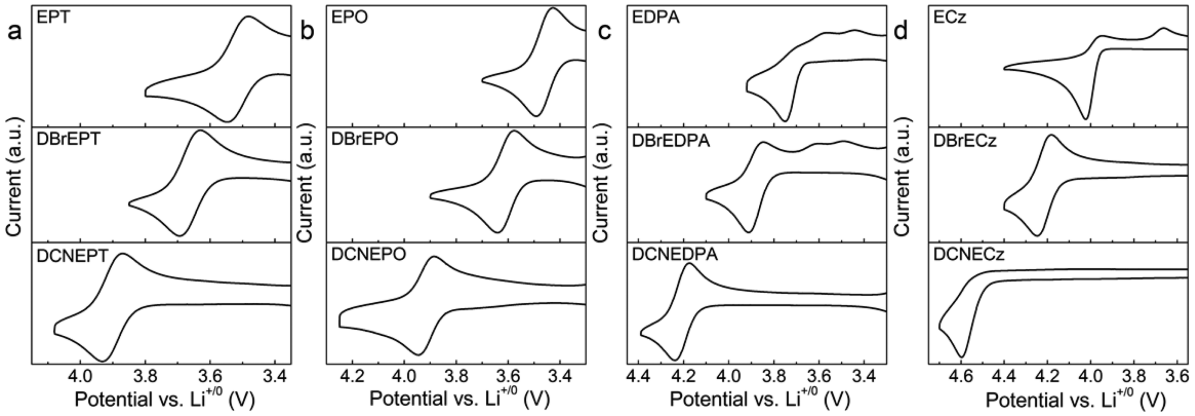

Figure 3. Cyclic voltammograms of EPT and its derivatives (a), EPO and its derivatives (b), EDPA and its derivatives (c), and ECz and its derivatives (d) at 0.3 mM in 1.2 M LiPF$_6$ in EC/EMC (3:7) vs Li$^{+/0}$ at 0 V. All solutions contain Cp$_2$Fe as the internal reference (not shown, see Supporting Information for complete plots) and were recorded at 100 mV/s.

Glassy carbon was used as the working electrode, platinum wire as the counter electrode, and freshly anodized Ag/AgCl as the reference electrode. Ferrocene (Cp$_2$Fe) was added to each sample as an internal standard. CV was also performed in the battery electrolyte in an argon-filled glovebox, 1.2 M LiPF$_6$ in EC/EMC (3:7 wt %), with glassy carbon as the working electrode, platinum as the counter electrode, and lithium as the reference electrode. Ferrocene (Cp$_2$Fe) was added as an internal standard at ca. 0.3 mM, and peaks were referenced to Li$^{+/0}$ at 0 V. All voltammograms for determining oxidation potentials were recorded at scan rates of 100 mV/s, and multiple scans were performed for each sample. Voltammograms of compounds displaying reversible oxidations were also recorded at 0.3 and 0.05 M in battery electrolyte at scan rates (υ) ranging between 5 and 500 mV s^{-1} in order to obtain diffusion coefficients (D) of the neutral and oxidized species.

DFT Calculations. DFT calculations were performed with Gaussian 09.[29] Molecular geometries were optimized first by the semiempirical quantum chemical method PM3.[30] Then density functional theory (DFT) was used for further optimization of geometry using Becke's three-parameter exchange functional (B3)[31] in combination with Lee, Yang, and Parr's (LYP)[32] correlation functions on the basis set of 6-31G(dp). Calculations were performed in the gas phase for neutrals (B3LYP) and for radical cations (UB3LYP) where an unrestricted formalism was applied. Adiabatic ionization potentials (IP) were obtained in the gas phase from the total energy differences between the optimized structures of neutral and charged (radical cation) species.

Generation and Spectroscopic Analysis of Radical Cations. Samples for UV−vis spectroscopy were prepared in optical glass cuvettes (Starna), and spectra were obtained using an Agilent 8453 diode array spectrometer. The analyte was dissolved in anhydrous dichloromethane (1.71×10^{-4} M) in a vial, and 2.9 mL of solution was transferred to a cuvette with a 1 cm path length. A freshly prepared solution of TDBPA$^{\bullet+}$ oxidant (100 μL, 4.5×10^{-3} M in dichloromethane) was added using a Hamilton syringe, and the cuvette was immediately capped with a Teflon stopper and rotated to distribute the oxidant throughout the sample. Assuming complete electron transfer, unless otherwise noted, this reaction results in a net concentration of 1.5×10^{-4} M in radical cation, 1.5×10^{-4} M in the neutral form of the oxidizing agent, and 1.5×10^{-5} M in unreacted, neutral redox shuttle. Numerous spectra were obtained at various times up to 5 h after radical cation generation.

Battery Fabrication and Cycling. All battery electrolyte components—ethylene carbonate, ethyl methyl carbonate, and lithium hexafluorophosphate—were battery grade and were purchased from BASF Corporation (Florham Park, NJ). Overcharge tests were conducted with 2032 coin cells using LiFePO$_4$ (Piotrek, Japan) as the cathode and synthetic graphite

dx.doi.org/10.1021/jp503767h | J. Phys. Chem. C 2014, 118, 14824−14832

Table 1. Calculated Adiabatic IPs and Half-Wave Oxidation Potentials ($E^{+/0}_{1/2}$) vs $Cp_2Fe^{+/0}$ in 0.1 M nBu_4NPF_6 in DCM and vs $Li^{+/0}$ in 1.2 M $LiPF_6$ in EC/EMC (3:7)[a]

compound	calcd adiabatic IP (eV)	$E^{+/0}_{1/2}$ vs $Cp_2Fe^{+/0}$ (V) for 0.3 mM redox shuttle	$E^{+/0}_{1/2}$ vs $Li^{+/0}$ (V) for 0.3 mM redox shuttle	$E^{+/0}_{1/2}$ vs $Li^{+/0}$ (V) with 0.05 M redox shuttle	$D_N \times 10^{-6}$ for 0.3 mM redox shuttle	$D_N \times 10^{-6}$ for 0.05 M redox shuttle
EPT	6.37	0.27	3.51	3.52	2.3	1.3
DBrEPT	6.60	0.41	3.66	3.67	2.4	1.1
DCNEPT	7.20	0.66	3.90	3.91	2.7	0.8
EPO	6.17	0.21	3.46	3.46	3.3	1.3
DBrEPO	6.41	0.37	3.61	3.62	3.4	1.1
DCNEPO	7.06	0.67	3.91	3.92	3.9	0.8
EDPA	6.50	0.46[b] (0.34, 0.19)	3.67[b] (3.60, 3.46)	–[e]	–[e]	–[e]
DBrEDPA	6.67	0.63[c] (0.41, 0.27)	3.88[c] (3.64, 3.52)	–[e]	–[e]	–[e]
DCNEDPA	7.36	0.97	4.21	4.22	1.6	0.9
ECz	6.89	0.73[b] (0.49)	3.99[b] (3.71)	–[e]	–	–[e]
DBrECz	7.02	0.98	4.22	4.23[b]	4.5	–[e]
DCNECz	7.73	1.37[d]	4.57[d]	4.61[c]	2.0	–[e]

[a]Values in parentheses are additional peaks observed at reverse scan after oxidation. [b]Irreversible. [c]Reversible only at scan rates of 300 mV/s and higher. [d]Irreversible in the presence of Cp_2Fe. [e]Not reported because oxidation was not reversible.

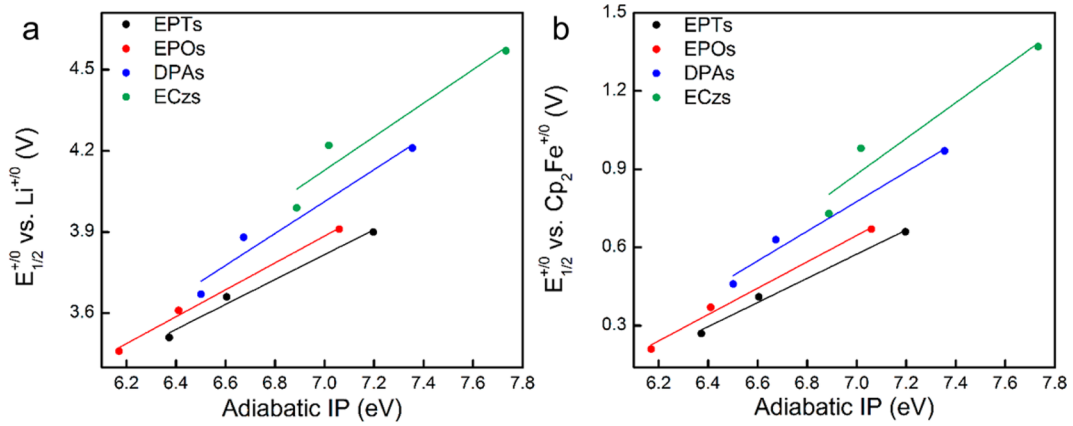

Figure 4. Plots of the oxidation potentials vs $Cp_2Fe^{+/0}$ of redox shuttle candidates vs calculated adiabatic IPs (a) and oxidation potentials vs $Li^{+/0}$ vs the calculated adiabatic IPs, both grouped by type of core and shown with lines of best fit.

(Gen-2, Argonne National Laboratory) as the anode. Gen-2 anode is composed of 92 wt % MAG-10 graphite (Hitachi) as the active material and 8 wt % poly(vinylidene fluoride) (PVDF) as the binder. The electrolyte was 1.2 M $LiPF_6$ in EC/EMC (3:7 wt %). Coin cells were prepared in an argon-filled glovebox. A Maccor 4200 battery cycler was used for performing the cycling procedure. The coin cells were charged with constant current C/10 for 20 h (100% overcharge) or until a specific upper voltage (5.0 V) was reached. If the voltage of the coin cell did not reach 5.0 V after 20 h, the charging step was followed by a 30 s rest followed by discharging to 3.0 V with constant current of C/10. Cycling of coin cells that reached 5.0 V and/or dropped below 3.0 V was stopped.

3. RESULTS AND DISCUSSION

Electronic Properties. Cyclic voltammetry (CV) experiments were performed to determine oxidation potentials in acetonitrile (ACN) containing 0.1 M nBu_4NPF_6 and in ethylene carbonate/ethyl methyl carbonate (EC/EMC, 3:7 wt %) containing 1.2 M $LiPF_6$. The voltammograms are shown in Figures 2 and 3, respectively. Expanded versions containing the internal reference Cp_2Fe are shown in the Supporting Information (Figures S5 and S6). All EPT (Figures 2a and 3a) and EPO (Figures 2b and 3b) compounds exhibited reversible oxidation in both electrolytes, whereas reversibility of oxidation for EDPA (Figures 2c and 3c) and ECz (Figures 2d and 3d) compounds varied with the substituent.

As expected, the oxidation potentials of the diarylamine derivatives increased (shifted anodically) with increased electron-withdrawing strength of the substituents (−Br and −CN). The reversibility of the redox process for EDPA derivatives (Figures 2c and 3c) and ECz derivatives (Figures 2d and 3d) suffered in both electrolytes, showing that in some cases although we had blocked the positions *para* to the N atom to decrease the likelihood for dimerization, the stability of the radical cations—based on the irreversibility of the oxidations in the voltammograms—was poorer than that of their unsubstituted parent compounds. The oxidation potentials of EPT and EPO derivatives are lower than those of their ECz counterparts due to the electron-rich sulfur and oxygen atoms. The presence of polarizable heteroatoms within the conjugated framework usually lowers ionization potentials relative to their hydrocarbon counterparts.[33,34] The oxidation potentials of the EDPA derivatives, as expected, are likewise lower than those of ECz derivatives. The relatively high oxidation potentials exhibited by carbazole derivatives may be due to the enhanced conjugation of the planar carbazole core, an attribute that resulted in decreased HOMO energy.

dx.doi.org/10.1021/jp503767h | J. Phys. Chem. C 2014, 118, 14824−14832

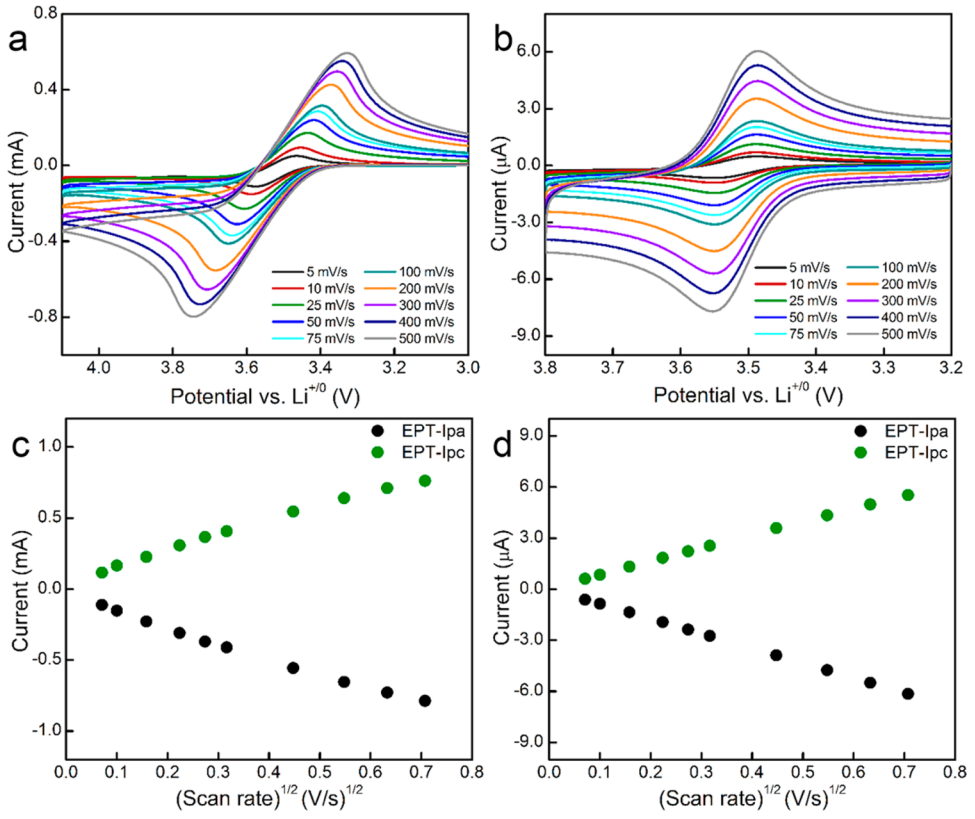

Figure 5. Cyclic voltammograms of 0.3 mM EPT (a) and 0.05 M EPT (b) in 1.2 M $LiPF_6$ in EC/EMC (3:7) vs $Li^{+/0}$ at 0 V at scan rates from 5 to 500 mV/s. Randles–Sevcik plots peak current vs square root of the scan rate for 0.3 mM EPT (c) and 0.05 M EPT (d).

Following oxidation, two new peaks appeared in the reverse scan of EDPA (0.34 and 0.19 V vs $Cp_2Fe^{+/0}$ at 0 V; 3.60 and 3.46 V vs $Li^{+/0}$ at 0 V) and DBrEDPA (0.41 and 0.27 V vs $Cp_2Fe^{+/0}$ at 0 V; 3.64 and 3.52 V vs $Li^{+/0}$ at 0 V) and are shown in Figures 2c and 3c for both electrolytes, respectively. These two peaks exhibited reversibility and increased in intensity in subsequent scans, consistent with the deposition of a new material on the surface of the working electrode. In contrast, DCNEDPA displayed no additional peak in the reverse scan upon its reversible oxidation. ECz exhibited an irreversible oxidation, and new peaks were observed in the reverse scan (0.49 V vs $Cp_2Fe^{+/0}$ at 0 V, Figure 2d; 3.71 V vs $Li^{+/0}$ at 0 V, Figure 3d), which became reversible with multiple scans. In contrast to the trends in the diphenylamine derivatives, DBrECz displayed reversible oxidation, whereas the oxidation of DCNECz was irreversible.

Electronic properties of the diarylamines were also studied by performing calculations using Gaussian 09.[29] Molecular geometries were optimized first by the semiempirical quantum chemical method PM3.[30] Density functional theory (DFT) was then applied for further optimization of geometry using the B3LYP[31,32] exchange correlation function with the basis set of 6-31G(dp). Adiabatic ionization potentials (IP) were obtained in the gas phase by calculating the total energy differences between the optimized structures of neutral and charged (radical cation) species. Electron contours in the highest occupied molecular orbital (HOMO) of each neutral and in the singly occupied molecular orbital (SOMO) of each charged species are listed in Figures S2 and S3 of the Supporting Information. The oxidation potentials of diarylamines vs $Cp_2Fe^{+/0}$ at 0 V and vs $Li^{+/0}$ at 0 V along with adiabatic IP are listed in Table 1.

A strong correlation, shown in Figure 4a, is evident in the oxidation potentials vs $Cp_2Fe^{+/0}$ at 0 V and adiabatic ionization potentials of the diarylamines within a type of aromatic core (such as in EPT derivatives or in EPO derivatives). Similarly, a strong correlation is also observed for the oxidation potentials vs $Li^{+/0}$ at 0 V and adiabatic ionization potentials, as shown in Figure 4b. The R^2 values for adiabatic IP vs experimental oxidation potentials vs $Cp_2Fe^{+/0}$ at 0 V and vs $Li^{+/0}$ at 0 V are listed in Table S2 of the Supporting Information.

CV experiments with different scan rates were performed in battery electrolyte for compounds that display reversible oxidation and diffusion coefficients were determined at 0.3 and 50 mM in redox shuttle. The peak currents during anodic and cathodic scan, *Ipa* and *Ipc*, respectively, at different sweep rates were used in the Randles–Sevcik equation[35,36]

$$Ip = (2.69 \times 10^5)n^{3/2}AD^{1/2}\upsilon^{1/2}C$$

in which *Ip* is peak current (A), *n* is the number of the electrons in the redox process ($n = 1$), *A* is the electrode area (cm^2), υ is scan rate (V/s), *C* is the shuttle concentration (mol cm^{-3}), and *D* is the diffusion coefficient (cm^2 s^{-1}). The oxidations of EDPA, DBrEDPA, ECz, and DCNECz are irreversible (Figure 3c,d). However, the oxidation of DCNECz is irreversible only in the presence of ferrocene; thus, it was also included in the diffusion coefficient study. Cyclic voltammograms of 0.3 mM EPT and 50 mM EPT at scan rates from 5 to 500 mV/s are shown in Figure 5a and 5b, respectively. And their Randles–Sevcik plots are shown in Figure 5c and 5d. Except for 50 mM DBrECz and 50 mM DCNECz, voltammograms and Randles–Sevcik plots of EPT (0.3 and 50 mM) were generally

dx.doi.org/10.1021/jp503767h | J. Phys. Chem. C 2014, 118, 14824–14832

Scheme 2. Schematic Representation of One-Electron Oxidation of EPT Derivatives with TDBPA$^{\bullet+}$

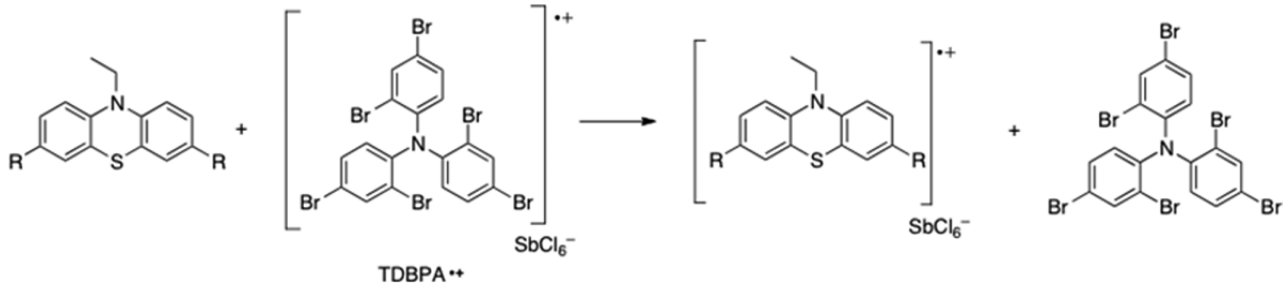

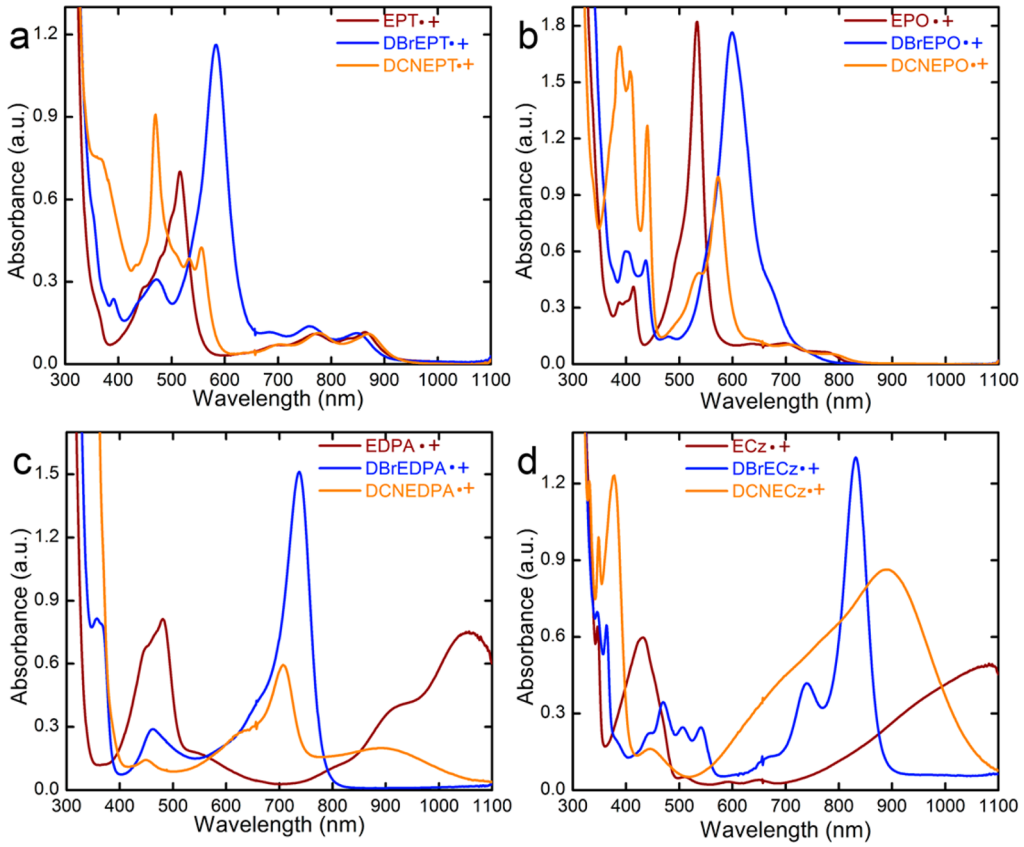

Figure 6. UV−vis absorption spectra of the radical cations of EPT and its derivatives (a), EPO and its derivatives (b), EDPA and its derivatives (c), and ECz and its derivatives (d) at 1.5×10^{-4} M in DCM immediately after generation with TDBPA$^{\bullet+}$.

representative of the general behavior of the redox shuttles, the remaining data for which are shown in Figures S7−S12.

The linearity of the plots of peak current vs square root scan rate from CVs collected at sweep rates between 5 and 500 mV/s suggests a diffusion-controlled reaction, and the slope of this plot was used to obtain the diffusion coefficients.[37] The diffusion coefficients of neutral species for all of the compounds with reversible oxidation are listed in Table 1, and those for the oxidized species and the ratio of oxidized to neutral species are shown in the Supporting Information (Table S3). The oxidized species have lower diffusion coefficients than their neutral counterparts, which may be due to stronger interactions of the oxidized molecule with the PF_6^- anion and carbonate solvents.[38] This interaction is more prominent at lower concentrations of analytes (0.3 mM) whereas the ratio of diffusion coefficient of oxidized species to reduced species (D_O/D_R) is higher at higher concentrations (50 mM), as shown in Table S3. The oxidation of DBrECz is irreversible at 0.05 M, and new peaks formation observed in voltammograms, even at higher scan rates (500 mV/s). The oxidation of DCNECz also shows diminished reversibility with decreasing scan rate. Thus, diffusion coefficients of DBRECz and DCNECz were not obtained at 0.05 M.

UV−vis Studies. To study the stability of the oxidized form of the redox shuttles, the decomposition of which is thought to be the main limiting factor in overcharge performance, we generated radical cations *in situ* using the oxidant tris(2,4-dibromophenyl)aminium hexachloroantimonate (TDBPA$^{\bullet+}$).[39] The schematic representation of one-electron oxidation for EPT derivatives is shown in Scheme 2. Recently, we found a general correlation between radical cation stability and the number of overcharge cycles reported for each compound and were curious if radical cation stability in dilute solutions is a reliable predictor of overcharge performance as the diversity of diarylamine cores and substituents is varied.[27]

dx.doi.org/10.1021/jp503767h | J. Phys. Chem. C 2014, 118, 14824−14832

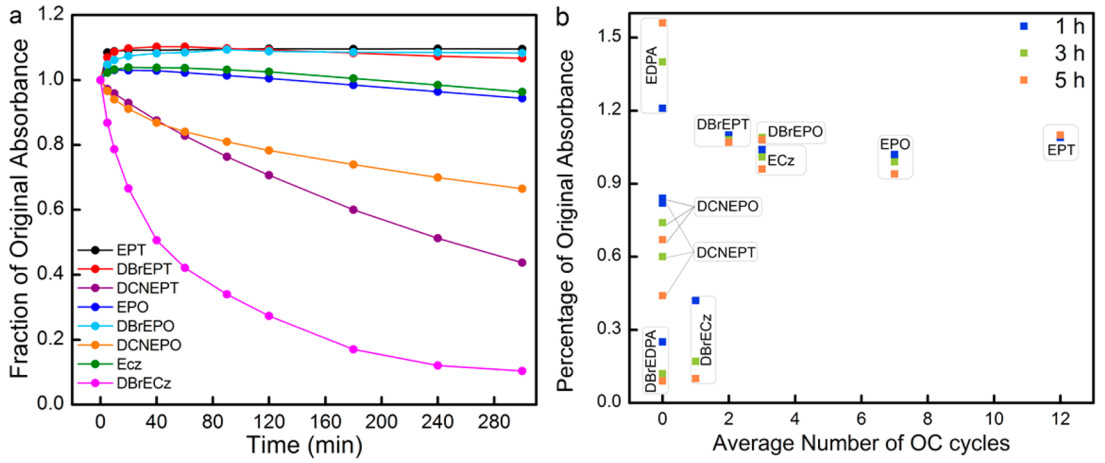

Figure 7. Normalized absorbance of the radical cations of diarylamines and their derivatives at the wavelength of maximum absorbance in visible region in DCM over 5 h (a) and the percentage of absorbance at the 1st, 3rd, and 5th h for redox shuttle candidates along with average number of overcharge cycles obtained with synthetic graphite/$LiFePO_4$ coin cell batteries (b).

Radical cations were generated at 0.15 mM (assuming complete electron transfer) using $TDBPA^{\bullet+}$, which was added to solutions of each redox shuttle candidate in dichloromethane (DCM), and stability was monitored using UV−vis spectroscopy. UV−vis spectra of the oxidized diarylamines and their derivatives show peaks that are red-shifted compared to the neutral forms (Figure 6a−d). This clear distinction of the radical cation absorption features allowed us to monitor the absorbance of the radical cations over time. Specifically, we monitored the intensity of each radical cation at the maximum absorbance in the visible region. The wavelengths monitored for determining relative concentration of oxidized redox shuttle candidates are listed in the Supporting Information (Table S4). Figure 7a shows a plot of the normalized absorbance of the radical cations over 5 h, averaged over three runs in DCM. Individual UV−vis absorption spectra of each radical cation in DCM for 5 h are shown in Figures S13−S16. While most radical cations showed peaks that diminished over time, but with the same overall spectral features, the EDPA group was an exception. For example, the radical cations of DCNEDPA disappeared in the first 5 min (Figure S15d), revealing low stability of this species. In the case of DBrEDPA, radical cations showed multiple peaks emerging with different behavior, suggesting that oxidation leads to one or more reaction pathways. The high oxidation potential of DCNECz prevented its oxidation with $TDBPA^{\bullet+}$, so we were unable to study its radical cation stability using this chemical oxidant.

The stability of the radical cation can be used to identify candidates for extended overcharge performance because it is the more reactive of the two active oxidation states of the redox shuttle. However, stable radical cations do not guarantee extended overcharge performance. Differences in conditions from dilute DCM to the battery environment involve changes in redox shuttle concentration, a different solvent (carbonates), an electrolyte salt (i.e., $LiPF_6$), encounters with electrode and polymer separator surfaces, and an electric field. Thus, far we have used radical cation stability as a way to weed out unstable radical cations, bearing in mind that only some of the stable radical cations will show extended overcharge performance. Figure 7b shows a plot of the stability of the radical cations of diarylamines for 1, 3, and 5 h versus the average number of overcharge protection cycles obtained from coin cell experiments. As mentioned above, stable radical cations in dilute solutions in DCM do not guarantee a large number of overcharge protection cycles.

Because of the relative empirical character of the UV−vis decay data, the stabilities of the radical cations were compared to the stability of the EPT radical cation (represented as $EPT^{\bullet+}$), which is relatively stable, with little decay over 5 h. In fact, the absorbance of the EPT radical cation increases over 5 h, which is due to the oxidation of remaining neutral EPT by the solvent, as is often the case for electron rich amines in chlorinated solvents.

In the series of *N*-ethyldiarylamines, $EPT^{\bullet+}$ and $EDPA^{\bullet+}$ do not decay measurably in 5 h, whereas the decay of $EPO^{\bullet+}$ and $ECz^{\bullet+}$ is apparent although almost negligible. Of the dibrominated derivatives, $DBrEPT^{\bullet+}$ and $DBrEPO^{\bullet+}$ show similar stability to $EPT^{\bullet+}$, whereas DBrECz decays rapidly. The changes in the UV−vis spectra of $DBrEDPA^{\bullet+}$ (Figure S15c) indicate that other reactions—not simply decomposition to the neutral version of the compound—are occurring, producing either new radical cations or other conjugated species that absorb in the visible region. All tested dicyano derivatives decayed more rapidly than their parent molecules, indicating that the radical cations have lower stability.

Overcharge Protection Performance. Performance of the diarylamines as redox shuttles was tested in overcharge experiments in lithium-ion batteries. Coin cells were assembled containing diarylamines as electrolyte additives at 0.05 M in EC/EMC (3:7 wt %) containing 1.2 M $LiPF_6$. Cycling data for EPT, DBrEPT, and DCNEPT have been reported.[28] However, for consistency, in this work we tested the redox shuttles at lower concentrations due to the solubility constraints of some of the derivatives, specifically DCNEPT and DCNEPO. For direct comparison to EPT[10] and our previously reported DBrEPT and DCNEPT,[28] all compounds were tested at 0.05 M in case of variability in overcharge performance at different redox shuttle concentrations. The number of overcharge cycles and potential of overcharge protection are listed in Table 2 along with measured oxidation potentials vs $Li^{+/0}$ and calculated adiabatic IPs. Plots of voltage vs time for coin cell experiments are shown in Figures S17 and S18.

For EPT, EPO, and ECz derivatives, the number of overcharge protection cycles was higher with lower oxidation potentials, with nonsubstituted derivatives having more overcharge cycles than the dibrominated derivatives, which were in

dx.doi.org/10.1021/jp503767h | J. Phys. Chem. C 2014, 118, 14824−14832

Table 2. Half-Wave Oxidation Potentials ($E_{1/2}^{+/0}$) vs $Li^{+/0}$ in 1.2 M $LiPF_6$ in EC/EMC (3:7) (Values in Parentheses Are New Peaks Observed on Subsequent Scans), Potential for Overcharge Protection, and the Number of Overcharge Cycles Obtained as Well as a Comparison to Radical Cation Stability Results: Ratio of the Absorbance at 5th h to That of the Initial Absorbance

compound	$E_{1/2}^{+/0}$ vs $Li^{+/0}$ (V)	potential of overcharge protection vs $Li^{+/0}$ (V)	no. of OC cycles from individual coin cells and average (in parentheses)	ratio of abs at 5th h to the original abs
EPT	3.51	3.5	1, 14, 21 (12)	1.10
EPO	3.46	3.4	3, 7, 11 (7)	0.99
ECz	3.99[a] (3.71)	3.4−3.7	0, 2, 7 (3)	0.96
DBrEPT	3.66	3.6	0, 2, 4 (2)	1.08
DBrEPO	3.61	3.6	3, 3, 2 (3)	1.09
DBrECz	4.22	3.4	0, 0, 3 (1)	0.10
DCNEPT	3.90	–	0, 0, 0 (0)	0.60
DCNEPO	3.91	–	0, 0, 0 (0)	0.78
EDPA	3.67[a] (3.60, 3.46)	–	0, 0, 0 (0)	1.60
DBrEDPA	3.88[b] (3.64, 3.52)	–	0, 0, 0 (0)	0.09
DCNEDPA	4.21	–	0, 0, 0 (0)	0.01
DCNECz	4.57	–	0, 0, 0 (0)	N/A

[a]Irreversible. [b]Reversibility is scan rate related.

turn more protecting than the dicyano derivatives, which showed no overcharge protection in these conditions.

Despite varying radical cation stabilities, none of the *N*-ethyldiphenylamine compounds (EDPA, DBrEDPA, and DCNEDPA) exhibited overcharge protection. The greater stability of EPT and EPO derivatives in comparison to corresponding ECz and EDPA derivatives could be due to the electron-donating effect of the S and O atoms into the aromatic rings of EPT and EPO, respectively, stabilizing the positive charge of the radical cation. Additionally, EDPA may be less stable than the fused cores because it has additional open *ortho* positions, which provide more sites for reaction. In DBrECz batteries, the potential for overcharge protection varies from about 3.4 V, which is significantly lower than the oxidation potential from cyclic voltammetry. This may be due to electropolymerization, producing a lower oxidation potential poly(ECz), dropping the voltage of overcharge protection. Similarly, while DBrEPT's potential for overcharge protection initially matches its oxidation potential, with time the potential for overcharge protection drops by at least 0.5 V, consistent with the formation of poly(EPT).

4. CONCLUSIONS

In summary, diarylamine derivatives were synthesized and were studied as redox shuttle candidates for overcharge protection in LIBs with high voltage cathodes. Their oxidation potentials were determined using cyclic voltammetry, which correlated well with trends in adiabatic IPs calculated using density functional theory. Radical cation stability at low concentrations (1.5×10^{-4} M) in DCM was consistent with overcharge performance for the case of unstable radical cations, which did not exhibit overcharge protection, but stability of radical cations in dilute solutions (1.5×10^{-4} M) does not guarantee that the additives will protect from overcharge at higher (0.05 M) concentrations. As we anticipated, the incorporation of electron-withdrawing substituents correlates with a smaller number of the overcharge cycles. While DFT calculations can be used to predict oxidation potentials, which will be useful in the identification of redox shuttle candidates for high voltage cathodes, it is important to note that predicting reactivity is far more difficult. A challenge and opportunity exists to identify kinetically stable redox shuttles *prior* to their synthesis and testing: a complicated task given the variety of pathways of decomposition possible at high concentrations in battery electrolyte. We look forward to continued optimization of screening techniques of candidates for overcharge as well as the identification of decomposition products of their radical cations to enable us to learn more about reactivity of these electron-deficient species in our search for stable, high voltage redox shuttles.

■ ASSOCIATED CONTENT

Supporting Information

Experimental details for synthesis, UV−vis, cyclic voltammetry, X-ray crystallographic data, highest occupied molecular orbitals of neutral and singly occupied molecular orbitals of radical cations, and extended voltammograms in both electrolytes. This material is available free of charge via the Internet at http://pubs.acs.org.

■ AUTHOR INFORMATION

Corresponding Author

*E-mail susan.odom@uky.edu; Tel +00-(1)-859-257-3294; Fax 00-(1)-859-323-9985 (S.A.O.).

Notes

The authors declare no competing financial interest.

■ ACKNOWLEDGMENTS

Acknowledgment is made to the donors of the American Chemical Society Petroleum Research Fund for support of this research through a Doctoral New Investigator Award, the National Science Foundation Division of Chemistry (CSDM-B) under Award Number CHE-1300653, and the University of Kentucky's Office of the Vice President for Research and the College of Arts & Sciences for start-up funding. We thank the University of Kentucky's High Performance Computing Facility for supercomputer access. At Argonne National Laboratory, we thank Bryant Polzin and Andrew Jansen from the Cell Analysis, Modeling, and Prototyping Facility for providing electrodes and battery cycler components. We thank Simon Jones at Contour Energy Systems for coin cell supplies.

■ REFERENCES

(1) Dahn, J.; Jiang, J.; Moshurchak, L.; Buhrmester, C.; Wang, R. L. The Drugstore Li-Ion Cell. *Electrochem. Soc. Interface* **2005**, *14*, 27−31.

(2) Oh, B.; Amine, K. Evaluation of Macromonomer-Based Gel Polymer Electrolyte for High-Power Applications. *Solid State Ionics* **2004**, *175*, 785−788.

(3) Wen, J. W.; Yu, Y.; Chen, C. H. A Review on Lithium-Ion Batteries Safety Issues: Existing Problems and Possible Solutions. *Mater. Express* **2012**, *2*, 197−212.

(4) Lee, D.-Y.; Lee, H.-S.; Kim, H.-S.; Sun, H.-Y.; Seung, D.-Y. Redox Shuttle Additives for Chemical Overcharge Protection in Lithium Ion Batteries. *Korean J. Chem. Eng.* **2002**, *19*, 645−652.

(5) Richardson, T. J.; Ross, P. N., Jr. *In situ* UV−Visible Spectroscopy: Characterization of Overcharge Protection Additives for Secondary Lithium Batteries. *J. Power Sources* **1999**, *84*, 1−5.
(6) Thomas-Alyea, K. E.; Newman, J.; Chen, G.; Richardson, T. J. Modeling the Behavior of Electroactive Polymers for Overcharge Protection of Lithium Batteries. *J. Electrochem. Soc.* **2004**, *151*, A509−A521.
(7) Shima, K.; Shizuka, K.; Ue, M.; Ota, H.; Hatozaki, T.; Yamaki, J. Reaction Mechanisms of Aromatic Compounds as an Overcharge Protection Agent for 4 V Class Lithium-Ion Cells. *J. Power Sources* **2006**, *161*, 1264−1274.
(8) Adachi, M.; Tanaka, K.; Sekai, K. Aromatic Compounds as Redox Shuttle Additives for 4 V Class Secondary Lithium Batteries. *J. Electrochem. Soc.* **1999**, *146*, 1256−1261.
(9) Chen, J.; Buhrmester, C.; Dahn, J. R. Chemical Overcharge and Overdischarge Protection for Lithium-Ion Batteries. *Electrochem. Solid-State Lett.* **2005**, *8*, A59−A62.
(10) Buhrmester, C.; Moshurchak, L. M.; Wang, R. L.; Dahn, J. R. Phenothiazine Molecules Possible Redox Shuttle Additives for Chemical Overcharge and Overdischarge Protection for Lithium-Ion Batteries. *J. Electrochem. Soc.* **2006**, *153*, A288−A294.
(11) Buhrmester, C.; Moshurchak, L. M.; Wang, R. L.; Dahn, J. R. The Use of 2,2,6,6-Tetramethylpiperinyl-Oxides and Derivatives for Redox Shuttle Additives in Li-Ion Cells. *J. Electrochem. Soc.* **2006**, *153*, A1800−A1804.
(12) Moshurchak, L. M.; Buhrmester, C.; Wang, R. L.; Dahn, J. R. Comparative Studies of Three Redox Shuttle Molecule Classes for Overcharge Protection of $LiFePO_4$-Based Li-Ion Cells. *Electrochim. Acta* **2007**, *52*, 3779−3784.
(13) Yurchenko, O.; Freytag, D.; Zur Borg, L.; Zentel, R.; Heinze, J.; Ludwigs, S. Electrochemically Induced Reversible and Irreversible Coupling of Triarylamines. *J. Phys. Chem. B* **2012**, *116*, 30−39.
(14) Zhang, L.; Zhang, Z.; Wu, H.; Amine, K. Novel Redox Shuttle Additive for High-Voltage Cathode Materials. *Energy Environ. Sci.* **2011**, *4*, 2858−2862.
(15) Chen, Z.; Amine, K. Bifunctional Electrolyte Additive for Lithium-Ion Batteries. *Electrochem. Commun.* **2007**, *9*, 703−707.
(16) Moshurchak, L. M.; Lamanna, W. M.; Bulinski, M.; Wang, R. L.; Garsuch, R. R.; Jiang, J. W.; Magnuson, D.; Triemert, M.; Dahn, J. R. High-Potential Redox Shuttle for Use in Lithium-Ion Batteries. *J. Electrochem. Soc.* **2009**, *156*, A309−A312.
(17) Moshuchak, L. M.; Bulinski, M.; Lamanna, W. M.; Wang, R. L.; Dahn, J. R. Direct Comparison of 2,5-Di-*tert*-butyl-1,4-dimethoybenzene and 4-*tert*-butyl-1,2-dimethoxybenzene as Redox Shuttles in $LiFePO_4$-Based Li-Ion Cells. *Electrochem. Commun.* **2007**, *9*, 1497−1501.
(18) Taggougui, M.; Carré, B.; Willmann, P.; Lemordant, D. 2,5-Difluoro-1,4-dimethoxybenzene for Overcharge Protection of Secondary Lithium Batteries. *J. Power Sources* **2007**, *174*, 1069−1073.
(19) Dantsin, G.; Jambunathan, K.; Ivanov, S. V.; Casteel, W. J.; Amine, K.; Liu, J.; Jansen, A. M.; Chen, Z. Advanced Electrolyte Salts with Inherent Overcharge Protection for Lithium Ion Batteries. Paper 223, Presented at the Meeting of The Electrochemical Society, Los Angeles, CA, October 16−21, 2005.
(20) Xu, W.; Chen, X.; Ding, F.; Xiao, J.; Wang, D.; Pan, A.; Zheng, J.; Li, X. S.; Padmaperuma, A. B.; Zhang, J.-G. Reinvestigation on the State-of-the-Art Nonaqueous Carbonate Electrolytes for 5 V Li-Ion Battery Applications. *J. Power Sources* **2012**, *213*, 304−314.
(21) Tarascon, J. M.; Armand, M. Issues and Challenges Facing Rechargeable Lithium Batteries. *Nature* **2001**, *414*, 359−367.
(22) Patoux, S.; Daniel, L.; Bourbon, C.; Lignier, H.; Pagano, C.; Cras, F. L.; Jouanneau, S.; Martinet, S. High Voltage Spinel Oxides for Li-Ion Batteries: From the Material Research to the Application. *J. Power Sources* **2009**, *189*, 344−352.
(23) Hu, M.; Pang, X. L.; Zhou, Z. Recent Progress in High-Voltage Lithium Ion Batteries. *J. Power Sources* **2013**, *237*, 229−242.
(24) Ambrose, J. F.; Carpenter, L. L.; Nelson, R. F. Electrochemical and Spectroscopic Properties of Cation Radicals: III. Reaction Pathways of Carbazolium Radical Ions. *J. Electrochem. Soc.* **1975**, *122*, 876−894.
(25) Moshurchak, L. M.; Buhrmester, C.; Dahn, J. R. Triphenylamines as a Class of Redox Shuttle Molecules for the Overcharge Protection of Lithium-Ion Cells. *J. Electrochem. Soc.* **2008**, *155*, A129−A131.
(26) Prudhomme, D. R.; Wang, Z.; Rizzo, C. J. An Improved Photosensitizer for the Photoinduced Electron-Transfer Deoxygenation of Benzoates and *m*-(Trifluoromethyl)benzoates. *J. Org. Chem.* **1997**, *62*, 8257−8260.
(27) Odom, S. A.; Ergun, S.; Poudel, P. P.; Parkin, S. R. A Fast, Inexpensive Method for Predicting Overcharge Performance in Lithium-Ion Batteries. *Energy Environ. Sci.* **2014**, *7*, 760−767.
(28) Ergun, S.; Elliott, C. F.; Kaur, A. P.; Parkin, S. R.; Odom, S. A. Overcharge Performance of 3,7-Disubstituted *N*-Ethylphenothiazine Derivatives in Lithium-Ion Batteries. *Chem. Commun.* **2014**, *50*, 5339−5341.
(29) Frisch, M. J.; et al. *Gaussian 09, Revision A.02*; Gaussian, Inc.: Wallingford, CT, 2009.
(30) Stewart, J. J. P. Optimization of Parameters for Semiempirical Methods I. Method. *J. Comput. Chem.* **1989**, *10*, 209−220.
(31) Becke, A. D. Density-functional Thermochemistry. III. The Role of Exact Exchange. *J. Chem. Phys.* **1993**, *98*, 5648−5652.
(32) Lee, C.; Yang, W.; Parr, R. G. Development of the Colle-Salvetti Correlation-Energy Formula into a Functional of the Electron Density. *Phys. Rev. B* **1988**, *37*, 785−789.
(33) Bueno, B.; Esteve, B.; Irurre, J.; Brillas, E.; Torelles, X.; Rius, J.; Alvarez-Larena, A.; Piniella, J. F.; Aleman, C.; Julia, L. Methyl- and Methoxy-substituted Di[1,4]benzodithiio[2,3-b:2,3-e]pyridines as New Electron Donor Compounds: Synthesis, Molecular Structure, Electrochemical Properties, and EPR Studies. *J. Chem. Soc., Perkin Trans. 2* **1999**, 1503−1512.
(34) Jorgensen, T.; Hansen, T. K.; Becher, J. Tetrathiafulvalenes as Building-Blocks in Supramolecular Chemistry. *Chem. Soc. Rev.* **1994**, *23*, 41−51.
(35) Randles, J. E B. A Cathode Ray Polarograph. Part II. The Current-Voltage Curves. *Trans. Faraday Soc.* **1948**, *44*, 327−338.
(36) Sevcik, A. Oscillographic Polarography with Periodical Triangular Voltage. *Collect. Czech. Chem. Commun.* **1948**, *13*, 349−377.
(37) Bard, A. J.; Faulkner, L. R. *Electrochemical Methods, Fundamentals and Applications*; Harris, D., Swain, E., Eds.; Wiley: New York, 1980; pp 226−260.
(38) Laoire, C. O.; Plichta, E.; Hendrickson, M.; Mukerjee, S.; Abraham, K. M. Electrochemical Studies of Ferrocene in a Lithium Ion Conducting Organic Carbonate Electrolyte. *Electrochim. Acta* **2009**, *54*, 6560−6564.
(39) The oxidation of the neutral form of oxidant tris(2,4-dibromophenyl)amine ($TDBPA^{\bullet+}$) is 4.39 V vs $Li^{+/0}$. See Figure S4 in the Supporting Information for its cyclic voltammograms in 1.2 M $LiPF_6$ in EC/EMC (3:7 wt %).